Electrical cell impedance spectral mesoscopic model applied to experimental data of variable size microelectrodes

Ana C. Buchini Labayen,[1,*] Mariela I. Bellotti,[1] Walter Bast,[2] and Fabian J. Bonetto[1,†]

[1]*Laboratorio de Cavitación y Biotecnología, Instituto Balseiro, Universidad Nacional de Cuyo/Comisión Nacional de Energía Atómica, San Carlos de Bariloche, Río Negro AGP8402, Argentina*

[2]*Laboratorio de Cavitación y Biotecnología, Comisión Nacional de Energía Atómica, San Carlos de Bariloche, Río Negro AGP8402, Argentina*

(Received 8 April 2021; accepted 14 March 2022; published 12 April 2022)

We apply the electric cell-substrate impedance sensing (ECIS) technique to monolayers of Madin-Darby canine kidney type II cells cultured on microelectrodes of different sizes. We analyze the effect of the microelectrode radius on the parameters provided by existing ECIS models. The cellular properties inferred from the models should be invariant to the change in the microelectrode radius used for the measurements, since these properties are inherent to the type of cells studied. The current standard model, the Giaever-Keese (GK) model, derived from electrical balances of a single cell extended to infinity by suitable boundary conditions, assumes an infinite microelectrode. The model is fitted to experimental data acquired with a large-radius microelectrode, which can be considered infinite for practical purposes. We compute the impedance of the other cell-covered microelectrodes from the parameters obtained with the GK model, resulting in values strongly discrepant with the experimental data for small microelectrodes. We repeat the process with the mean field (MF) model, an alternative model that depends on the microelectrode radius but not on the cell radius. In this paper we introduce the mesoscopic model, an analytical model that simultaneously includes the properties of an individual cell and the sizes of the microelectrode and the insulator (region between the microelectrode and the ground). The impedances calculated with the mesoscopic model are in excellent agreement with experimental data. Finally, the mesoscopic model reduces to the MF model when the insulator goes to infinity and to the GK model when it goes to zero.

DOI: 10.1103/PhysRevE.105.044401

I. INTRODUCTION

The electrical properties of biological tissues play an interesting role in understanding the basic underlying biological mechanisms involved in more complex processes, such as cancer development or embryogenesis. Although there exist techniques that allow the study of cellular electrical properties at the microscopic level, such as the patch clamp technique, a macroscopic approach is often preferred to characterize the behavior of tissues, since a microscopic description of the electrical response is complicated due to the variety of cells in a tissue and their distribution within it, and the heterogeneity of the properties of the tissue and the extracellular medium.

One of the techniques available for the study of tissues *in vitro* is electric cell-substrate impedance sensing (ECIS). It is an extremely sensitive and noninvasive technique that allows one to quantitatively evaluate morphological and functional properties of cells *in vitro* [1–4]. The characteristics and versatility of the ECIS technique allow its application in a wide variety of studies. It is a very useful tool in the analysis of processes that involve morphological changes in cells and the formation of cell-cell and cell-extracellular matrix interactions, such as cell differentiation, inflammatory processes, or tumor growth.

This technique is based on the measurements of electrical impedance that are performed exciting an electrode with ac signals of different frequencies. The gold electrode is composed of a microelectrode and a counter electrode contained on a biocompatible substrate (insulator). Adherent cells are cultured on the microelectrode, and the technique consists of measuring the impedance of the cell-free microelectrode (also called the naked microelectrode) and the impedance of the same microelectrode covered by the cells that restrict the flow of the current. The complete electrical response of the system at a given instant is determined by the behavior of the in-phase and out-of-phase voltages with respect to the excitation wave for all frequencies or by the resistance and capacitance of an in-series equivalent circuit.

Once the experimental data are obtained, a model allows us to estimate electrical and morphological significant quantities related to characteristics of the cells. The models use the measured impedance of a naked microelectrode to calculate the impedance of the cell-covered microelectrode as a function of the frequency, with a set of suitable morphological parameters. The model is then fitted to experimental data of the same covered microelectrode and the parameters are determined.

*ana.buchini@ib.edu.ar
†fabian.bonetto@ib.edu.ar

Since these morphological parameters are related to cellular properties inherent to the type of cell being studied, they should be independent of the experimental setup used to perform the measurements and remain invariable if the setup is modified. In particular, any model should provide the same set of parameters if the microelectrode radius is changed, since the cells grow on the substrate regardless of the size of the microelectrode it contains.

Given the relevance that the ECIS technique has acquired and its applicability in an extensive variety of studies, great efforts have been made to improve the experimental technique and the quality of the measurements. This has allowed us to carry out experiments with a microelectrode in a wide range of sizes, from very small, of sizes comparable to that of a cell, to very large, of a few millimeters in radius. It is for this reason that it is necessary to know the impact of the size of the microelectrode on the cellular properties that are estimated from the ECIS technique.

Ahuja *et al.* performed measurements with platinum naked microelectrodes of different sizes in a phosphate buffer solution electrolyte [5]; the effect of the microelectrode size on the sensitivity and frequency characteristics was studied by Lai *et al.* [6], who found a dependence of the optimal frequency for detection on the type of cell and the microelectrode size.

In this paper, the main objective is to analyze the effect of the microelectrode radius on the impedance of the cell-covered microelectrode calculated by four different models: the Giaever-Keese (GK) model [7], the Lo-Giaever-Keese (LGK) model [8], the mean field (MF) model [9], and the mesoscopic model, a model presented in this paper. We acquire the experimental data from Madin-Darby canine kidney type II (MDCK II) cell confluent homogeneous monolayers cultured on gold microelectrodes of different diameters in the range from 30 to 500 μm [10,11], manufactured in house on the top of a glass substrate [11].

We fit the models to the experimental data corresponding to the largest available microelectrode (500 μm diameter). With the parameters obtained and the experimental impedance of the other naked microelectrodes, we calculate the impedance of the covered microelectrodes with each model and compare it to the experimental data. We then fit the models to the experimental data corresponding to the different microelectrodes, finding a dependence of the parameters on the microelectrode radius.

We propose an alternative analytical model, the mesoscopic model. This model takes into account simultaneously the macroscopic behavior of the ECIS system, considering a cell monolayer which extends the coverage of the entire finite microelectrode and the finite insulator beyond, and its microscopic behavior, since the cell monolayer is modeled as a central cell surrounded by rings of cells whose properties are derived from those of a single cell, all electrically coupled to each other.

The mesoscopic model's description of the system includes both scales of the problem, in contrast to previous models, which just emphasize a unique scale. On the one hand, the GK and LGK models suppose that the microscopic behavior of the system dominates the general electrical response, as the electrical analysis is performed for a single cell adhered to the microelectrode and then extended to infinity, leading to the assumption of an infinite microelectrode. On the other hand, the MF model considers that the macroscopic behavior dominates the general electrical response, as it models a cell monolayer with mean electrical properties covering a finite microelectrode and an infinite insulator, without taking into account the individuality of the cells.

The three parameters considered by the mesoscopic model are related to biophysical properties of the cells. The parameters are the resistance of the intercellular junctions, the capacitance of the cell membrane, and a parameter related to the height of the space between the microelectrode surface and the basal membrane of the cell (cell-substrate space). The mesoscopic model is more general than the other models, as it contains them: It reduces to the GK model if no insulator is considered and to the MF model when the insulator is infinite.

II. EXPERIMENTAL PROCEDURES

A. Materials and methods

1. Electric cell-substrate impedance sensing technique

Figure 1(a) shows a schematic of the ECIS system and its electrical behavior. The system under study is composed of the microelectrodes, the counter electrode, the culture medium, and the cells analyzed. When this system is excited by the ac signal, its electrical behavior depends on the presence or absence of the cells on the microelectrode. The cells adhered to the microelectrode surface block the passage of current and therefore modify the electrical behavior that would show the same naked microelectrode (microelectrode in contact with the culture medium, with no cells on its surface). The ECIS technique consists of measuring the impedance of the naked and the covered microelectrode. The complete electrical response of the system at a given instant is determined by the behavior of the in-phase and out-of-phase voltages with respect to the excitation wave for all frequencies or by the resistance and capacitance of an in-series equivalent circuit.

We performed first the measurement of the impedance of the naked microelectrode and then that of the cell-covered microelectrode. The scan frequency data obtained were later analyzed using the ECIS models.

The experimental setup consisted of a function generator, a lock-in amplifier, a computer, and the electrode, as shown in the schematic of Fig. 1(b). We manufactured the electrode used containing gold microelectrodes of different diameters in the range from 30 to 500 μm and a counter electrode of 4 mm diameter. The microelectrodes were connected by gold thin leads to gold pads linked to the external electrical circuit. We placed the electrode into a holder that allowed the flat cable connection to the microelectrodes. A function generator excited a particular single microelectrode in series with a 1 MΩ load resistance, varying the frequency of the ac signal from 10 to 50 000 Hz in each measurement. The complex voltage was measured with a lock-in amplifier. Both the function generator and the lock-in were controlled by the computer. Our experimental setup allowed us to measure covered capacitances of the order of 80 pF for the smaller microelectrodes.

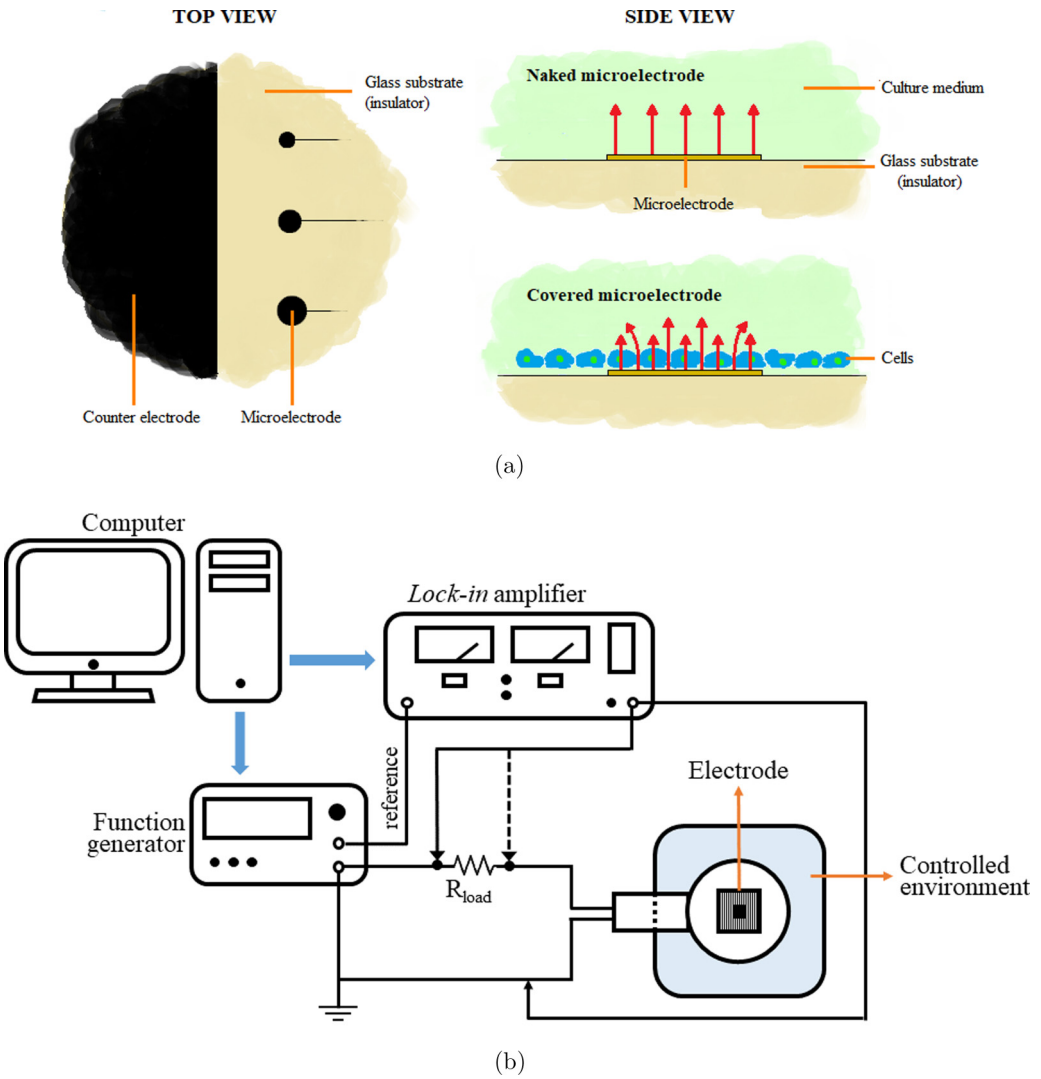

FIG. 1. (a) Schematic of the ECIS system and its electrical behavior. The drawings are not to scale: For the covered microelectrode, the thickness of the microelectrode is 0.05 μm, while the height of the cells is approximately 5 μm. (b) Schematic of the experimental setup.

2. *Microelectrodes*

We used a glass square plate of 25 × 25 × 1 mm^3 as substrate [11]. We spin coated the top of the substrate with a 5-μm-thick layer of photoresist. We developed the photoresist using ultraviolet light and a computer-generated mask containing circles of the microelectrode diameters (from 30 to 500 μm) and a large circle of the counter electrode diameter (4 mm) and removed the unwanted parts. We then sputtered a 50-nm-thick gold layer on top of the photoresist and substrate and used liftoff to remove the photoresist and the gold layer that was covering it. The active microelectrodes were the remaining circles of gold on top of the substrate, all forming part of a unique electrode. Each microelectrode was connected through a small gold lead to a 2-mm gold square pad, which electrically connect it to the external circuit.

The microelectrodes were designed to optimize the measurements, following the guidelines of reference [12], having a lead as short and thin as possible and with no photoresist on them to avoid the stray capacitance [13]. We also considered that the distance between the working and the counter microelectrodes does not affect the impedance measurements [14].

We plasma etched the electrode and then sterilized it in a dry oven at 120 °C for approximately 2 h. After that, we placed the electrode in a custom-made connection box in which all the microelectrodes and the counter electrode were electrically connected to a PC standard cable.

3. *Cell culture procedures*

We used an animal cell line to perform the measurements: MDCK II [10]. It was obtained from the Banco Argentino de Células.

We cultured the cells in sterile flasks (25 cm^2 Nalgene) and incubated at 37 °C in a humid environment (80%) with 5% concentration of CO_2 added to the air. We used modified Dulbecco (DMEM F-12, GIBCO) as the culture medium, supplemented with 10% fetal bovine serum (which mainly

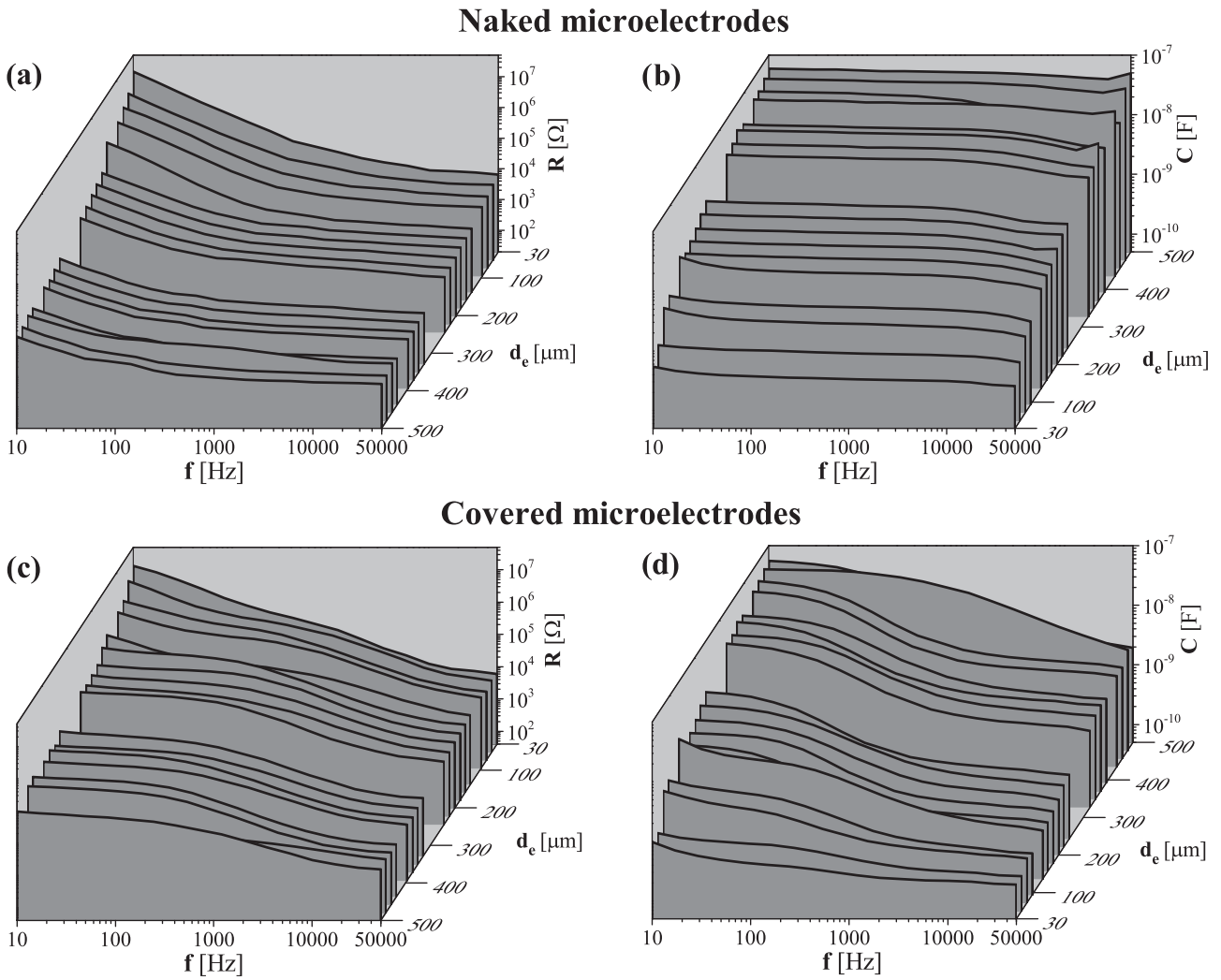

FIG. 2. Experimental data for monolayers of MDCK II cells cultured on microelectrodes of different diameters in the range from 30 to 500 μm: (a) resistance R and (b) capacitance C as a function of frequency f for different cell-free microelectrode diameters d_e and (c) resistance and (d) capacitance as a function of frequency for different cell-covered microelectrode diameters.

provides proteins and supplements that favor cell anchorage to the flask and to the microelectrodes), 1% antibiotic solution (penicillin, streptomycin, etc.), HEPES buffer, and 1% L-glutamine. We adjusted the final *p*H of the medium to a value of 7.4 with sodium hydroxide or hydrochloric acid as appropriate. We changed the complete culture medium approximately twice a week.

We examined daily the viability of the cells under the inverted light microscope and recorded the observations. When the cells reached confluence (of about 70% of the total surface of the flask), we trypsinated them, both for subculture purposes and for electrical properties measurements. We obtained the cell suspensions in the usual trypsination procedure (0.05 wt. % trypsin-EDTA 0.53 mM ^{4}Na).

We pretreated the microelectrodes with the proteins existing in the complete medium (serum), improving the cell attachment. We then seeded them with 0.5 ml of suspension at a cell concentration of 10^4–10^5 cells/ml.

B. Experimental data

Figure 2 plots the resistance R and the capacitance C as a function of frequency for different cell-free and cell-covered microelectrode diameters d_e. The sequence corresponds to diameters in the range from 30 to 500 μm [10]. All the microelectrodes were covered by the same MDCK II cell confluent homogenous monolayer, as they were part of a unique electrode placed in the micro-Petri dish where cells were cultivated. We repeated the measurements 6–10 times for each microelectrode, and the data shown are the median of each set of measurements.

We show in Fig. 3 the spectral resistance and capacitance of the naked and the covered microelectrodes with three different diameters. The circles represent the experimental data for the covered microelectrodes, while the squares correspond to the naked microelectrodes. In addition, black represents the data corresponding to the 30-μm-diam microelectrode, red to 201 μm, and blue to 500 μm. The spectral measurement was carried out for frequencies ranging from 10 to 50 000 Hz.

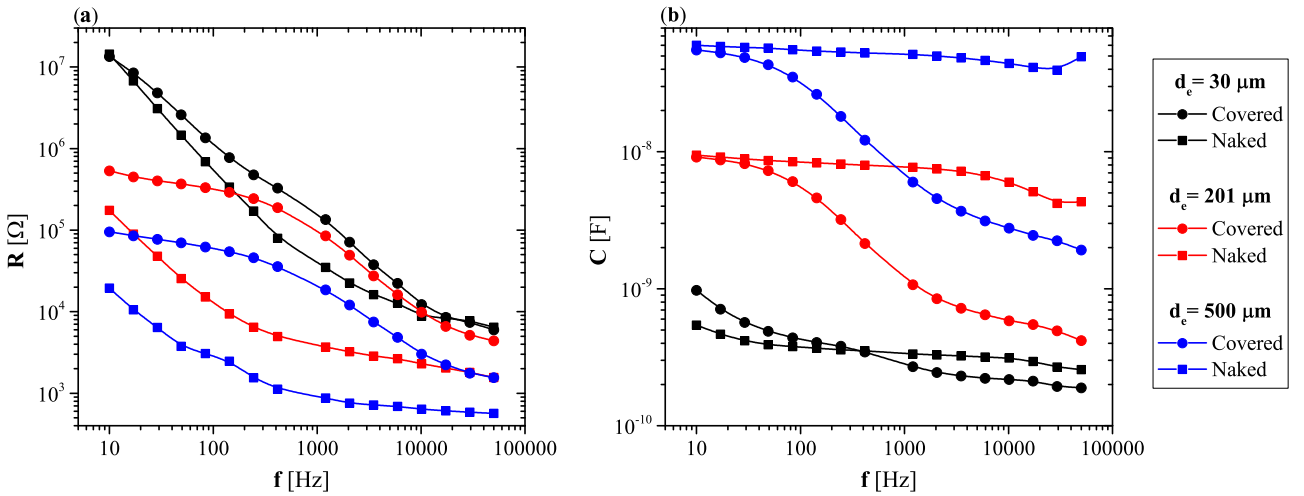

FIG. 3. Spectral (a) resistance and (b) capacitance of the naked (squares) and the covered (circles) microelectrodes with diameters of 30 μm (black), 201 μm (red), and 500 μm (blue).

Figure 4 shows the spectral resistance and capacitance for the naked (squares) and covered (circles) microelectrodes with a diameter of 500 μm and the fitting of the GK (red), MF (green), and mesoscopic (blue) models. We observe that the experimental data for the covered microelectrodes are above the estimates obtained with the models. We do not yet have an explanation for this effect, but it should be noted that it does not affect the conclusions of this work.

III. MESOSCOPIC MODEL

The ECIS problem has two scales: the cell radius (microscale) and the microelectrode radius (macroscale). Some previous ECIS models considered different scales of the problem.

The GK model (Fig. 5) and the LGK model consider that the microscopic behavior dominates the general electrical

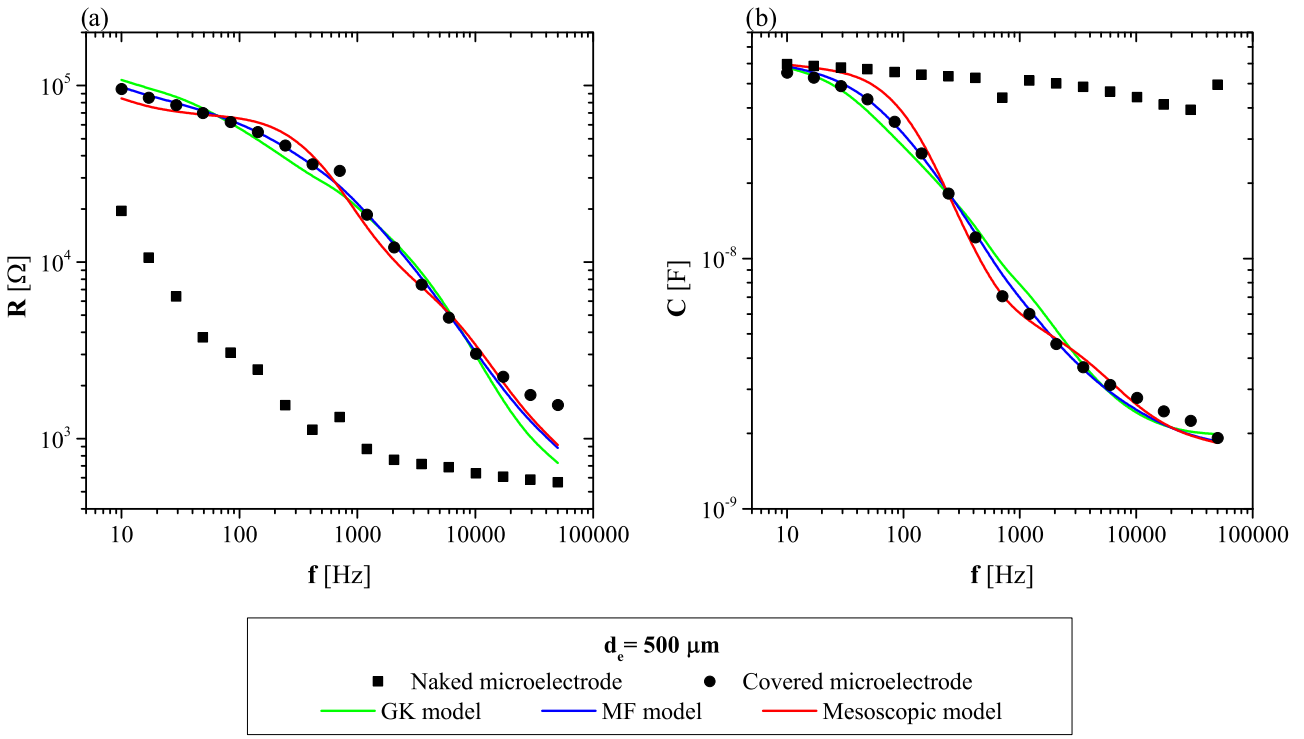

FIG. 4. Spectral (a) resistance and (b) capacitance of the naked (squares) and the covered (circles) microelectrode with a diameter of 500 μm of diameter and the fitting of the GK (red), MF (green), and mesoscopic (blue) models.

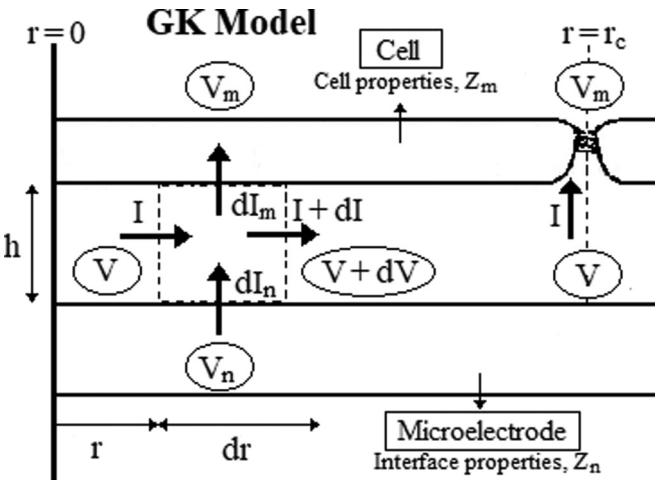

FIG. 5. Schematic of the system modeled by the GK model.

response. These models are based on the fact that the presence of a cell on a microelectrode blocks the current flow and therefore modifies the electrical behavior that the system would present in its absence. These models analyze the behavior of a single cell so that the modeled system consists of a disk-shaped cell adhered to the microelectrode. Electrical analysis is performed within the limits of this single cell and is extended to infinity by imposing suitable boundary conditions. By periodically extending the magnitudes to infinity, all the cells in a cell monolayer have the same boundary conditions, regardless of their position on the microelectrode. This means that the modeled microelectrode has no limits, so the model considers an infinite microelectrode.

In the GK model, the current passing through the microelectrode can flow in the radial direction in the space between the cell and the substrate (cell-substrate space) and can eventually flow into the cell through the basement membrane and exit through the apical membrane (transcellular pathway) or it can flow through the intercellular space and traverse the intercellular junction (paracellular pathway).

The LGK model is an extension of the GK model for epithelial cells, such as MDCK II. Cells of this type form monolayers with tighter and stronger intercellular junctions than endothelial cells and fibroblasts, so the resistance of the intercellular junctions is greater. Furthermore, one of its most important functions is ion diffusion, which is why endothelial cells have multiple pathways through which current can circulate that are not considered in the GK model. In the LGK model, once the current flows through the microelectrode, it can flow in the radial direction in the cell-substrate space and follow three main paths. There are two transcellular pathways: Current can flow into the cell through the basement membrane and out through the apical membrane or it can flow into the cell through the lateral membrane and out through the apical (this path is a consequence of the higher binding resistance that these cells present). The remaining pathway is paracellular: Current can flow through the intercellular space and traverse the intercellular junction.

The MF model (Fig. 6) is based on the fact that the presence of a cell monolayer on a microelectrode blocks the passage of current, changing the electrical behavior that the cell-free microelectrode would present. Although the model is obtained from a differential analysis of the problem, it considers that the macroscopic behavior dominates the general electrical response. The modeled system consists of a cell monolayer covering a finite microelectrode and an infinite insulator. This model analyzes the behavior of the entire cell monolayer, which has mean electrical properties due to the particular arrangement of the cells. The properties are characteristic of the monolayer, not of the cells, so the individuality of the cells is lost. In addition, since the modeled monolayer is also infinite, its properties are independent of the position, since all the points of the monolayer observe the same environment and there is radial symmetry. Again, the current that passes through the microelectrode can flow radially through the cell-substrate space and eventually cross the cell membranes of the monolayer. Beyond the limit of the microelectrode, the insulator does not provide current, so the current that flows through the cell-substrate space from the microelectrode region ends up crossing the cell monolayer. In this way, all the current leaving the microelectrode passes through the cell monolayer at some point.

In order to perform an analysis that considers microelectrodes and cells of any radius and any size insulator, we developed the mesoscopic model, which considers a finite

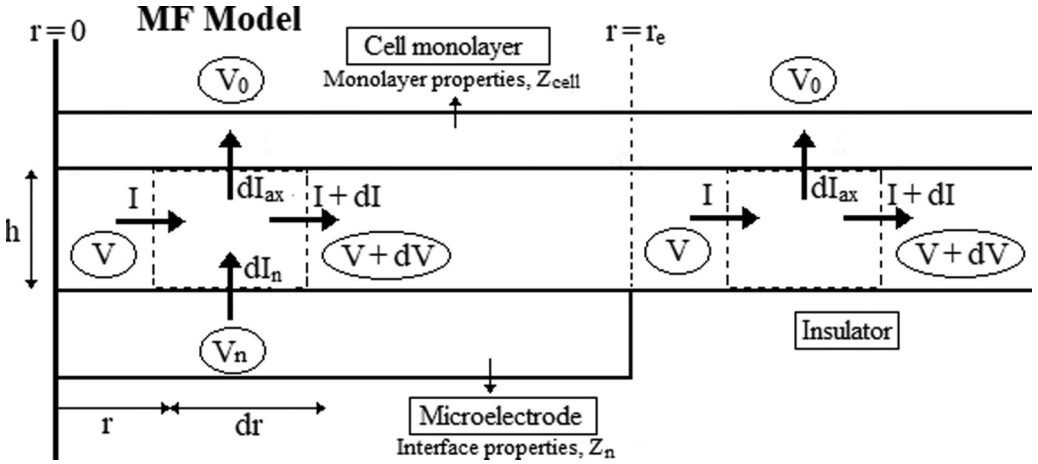

FIG. 6. Schematic of the system modeled by the MF model.

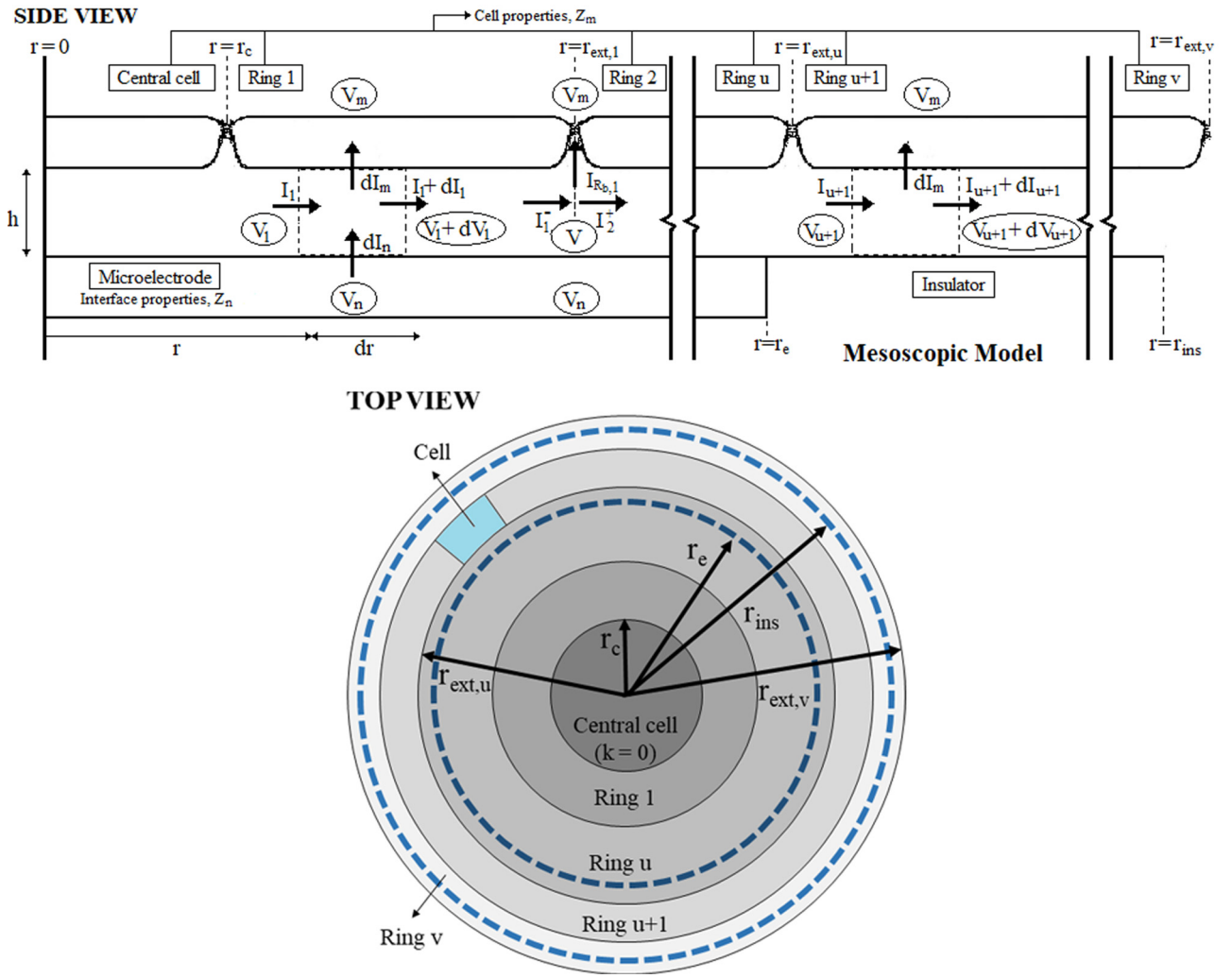

FIG. 7. Schematic of the system modeled by the mesoscopic model.

microelectrode covered by a cell monolayer formed by coupled individual cells, which also extends even beyond its limit on top of a finite insulator. Thus, our mesoscopic model includes simultaneously the microscopic and the macroscopic description of the problem and an insulator of finite size.

In this model, the system under analysis consists of a cell monolayer that covers a circular microelectrode surrounded by an insulator. As it is shown in the schematic of Fig. 7, this system is modeled as a microelectrode of radius r_e covered by a cell monolayer composed of a central cell of radius r_c surrounded by rings of cells electrically coupled to each other. The border conditions of each ring are generalizations of those of a single cell and the ring width is such that the area-perimeter ratio of an individual cell is preserved so that the junction resistance R_b (resistance by unit of area of the intercellular junctions) is compatible with that defined in the GK model.

The current that crosses the microelectrode can follow three different paths, whose relative importance depends on the specific impedance of the cell attached to the microelectrode and the resistance of the medium present in the cell-substrate space. It can flow through the cell membranes or through the cell-substrate space (in the radial direction, parallel to the substrate) and leave through the tight junctions or continue flowing towards the contiguous ring. The last path achieves the coupling between contiguous rings in this model. This path does not exist in the GK model, as the current between contiguous cells is null because of the symmetry in the border conditions that allows the extension of the electrical balances to infinity.

As in the MF model, cell rings extend beyond the limit of the microelectrode. There is no current supply from the substrate in this region and finally all the current flows through the monolayer. The difference is that the insulator (region between the microelectrode and the ground) is assumed to be infinite in the MF model, while the mesoscopic model considers a finite insulator. In the mesoscopic model, the insulator is modeled as a ring whose external radius is $r_{\text{ins}} = r_e + t_{\text{ins}}$, where t_{ins} is the width of the ring. Thus, the cell monolayer considered by the mesoscopic model does not have average electrical properties as in the MF model; being composed of cells coupled to each other, it has properties derived from the individual behavior of the cells that compose it, compatible with those described by the GK model.

The central cell and the rings are labeled with the index $k = 0, 1, \ldots, u, \ldots, v$, with 0 corresponding to the central

cell, 1 to the first ring, and so on; u to the last ring on the microelectrode; and v to the last ring on the insulator. The external radius of the kth ring is $r_{\text{ext},k}$.

The potential and current balances performed in the volumes limited by the dotted lines are of the same type as in the GK model. For the kth ring belonging to the region inside the microelectrode, the differential equation is

$$\frac{d^2V_k}{dr^2} + \frac{1}{r}\frac{dV_k}{dr} + \gamma_{\text{in}}^2 V_k + \beta_{\text{in}} = 0 \quad (0 \leqslant k \leqslant u), \tag{1}$$

where

$$\gamma_{\text{in}}^2 = \frac{\rho}{h}\left(\frac{1}{Z_n} + \frac{1}{Z_m}\right), \quad \beta_{\text{in}} = \frac{\rho}{h}\left(\frac{V_n}{Z_n} + \frac{V_m}{Z_m}\right), \tag{2}$$

and for the kth ring in the region outside the microelectrode, the equation is

$$\frac{d^2V_k}{dr^2} + \frac{1}{r}\frac{dV_k}{dr} + \gamma_{\text{out}}^2 V_k + \beta_{\text{out}} = 0 \quad (k > u), \tag{3}$$

where

$$\gamma_{\text{out}}^2 = \frac{\rho}{h}\frac{1}{Z_m}, \quad \beta_{\text{out}} = \frac{\rho}{h}\frac{V_m}{Z_m}. \tag{4}$$

Here $Z_n(f)$ is the specific impedance of the naked microelectrode (with f the frequency), $Z_m(f)$ is the specific impedance of the cells, V_m is the potential on the top of the cell monolayer, V_n is the applied potential, ρ is the resistivity of the culture medium, and h is the cell-substrate height. The specific impedance of the cells Z_m is modeled as purely capacitive, as the capacitance of the apical and basal cell membranes in series

$$Z_m = -\frac{i}{2\pi f \frac{C_m}{2}}, \tag{5}$$

where C_m is the capacitance of the cell membrane. We assume that the specific membrane resistance R_m of the cells is large compared to the reactance $\frac{1}{2\pi f C_m}$ at most frequencies. Since the resistance is in parallel with the reactance, it has little effect on the results. Thus, the potential beyond each ring is given by

$$V_k(r) = \begin{cases} C_k \mathscr{I}_0(\gamma_{\text{in}} r) + D_k \mathscr{K}_0(\gamma_{\text{in}} r) + \frac{\beta_{\text{in}}}{\gamma_{\text{in}}^2}, & 0 \leqslant k \leqslant u \\ C_k \mathscr{I}_0(\gamma_{\text{out}} r) + D_k \mathscr{K}_0(\gamma_{\text{out}} r) + V_m, & k > u, \end{cases} \tag{6}$$

where C_k and D_k are constants and $\mathscr{I}_0$ and $\mathscr{K}_0$ are the modified Bessel functions of zeroth order of the first and the second kind, respectively.

For the central cell of the layer, whose center coincides with the center of the microelectrode, the condition set is $I_0(0) = 0$. The boundary conditions for each ring and for the central cell are obtained by considering the continuity of the potential at the boundary

$$V_k(r_{\text{ext},k}) = V_{k+1}(r_{\text{ext},k}) \tag{7}$$

and the conservation of the current

$$\begin{aligned} I_k(r_{\text{ext},k}) = I_{k+1}(r_{\text{ext},k}) + I_{R_b,k} \Rightarrow & -\frac{2\pi h r_{\text{ext},k}}{\rho}\frac{dV_k}{dr}\bigg|_{r_{\text{ext},k}} \\ = & -\frac{2\pi h r_{\text{ext},k}}{\rho}\frac{dV_{k+1}}{dr}\bigg|_{r_{\text{ext},k}} + \frac{V_k(r_{\text{ext},k}) - V_m}{R_b} \\ & \times \pi\left[\left(\frac{r_{\text{ext},k+1} + r_{\text{ext},k}}{2}\right)^2 - \left(\frac{r_{\text{ext},k-1} + r_{\text{ext},k}}{2}\right)^2\right], \end{aligned} \tag{8}$$

where $I_{R_b,k}$ is the current that passes through the intercellular junction between the rings k and $k+1$. For the last ring on the insulator v,

$$\begin{aligned} I_v(r_{\text{ext},v}) = I_{R_b,v} \Rightarrow & -\frac{2\pi h r_{\text{ext},v}}{\rho}\frac{dV_v}{dr}\bigg|_{r_{\text{ext},v}} \\ = & \frac{V_v(r_{\text{ext},v}) - V_m}{R_b}\pi\left[r_{\text{ext},v}^2 - \left(\frac{r_{\text{ext},v-1} + r_{\text{ext},v}}{2}\right)^2\right]. \end{aligned} \tag{9}$$

The constants can be determined by solving the system of equations. Then the specific impedance Z_c of the cell-covered microelectrode can be established from

$$V_n - V_m = \frac{Z_c}{\pi r_e^2} I_n = \frac{Z_c}{\pi r_e^2}\int_0^{r_e} \frac{2\pi r}{Z_n}[V_n - V(r)]dr, \tag{10}$$

where I_n is the current going out the microelectrode. Thus,

$$Z_c = \frac{r_e^2 Z_n (V_n - V_m)}{\int_0^{r_e} 2r[V_n - V(r)]dr}. \tag{11}$$

The three parameters of this model are C_m, R_b and α, defined as $r_c(\frac{\rho}{h})^{1/2}$.

IV. RESULTS AND DISCUSSION

The Levenberg-Marquardt method for nonlinear parameter estimation was used to fit the models' parameters to the cell-covered experimental data. The constriction resistant (resistance of the solution) was considered equal to the value corresponding to the highest frequency of the measured resistance for a naked microelectrode. This resistance was subtracted from the measured resistance before fitting the models to the data and then added back for comparison with the experimental results. For all the calculations, the cell radius was $r_c = 7\ \mu$m [8] and the resistivity of the medium in the cell-substrate space was $\rho = 54\ \Omega$ cm (to compute h).

At first, we fitted the GK, LGK, MF, and mesoscopic models to the experimental data corresponding to the largest microelectrode available (500 μm diameter). This choice was due to the fact that the current standard model, the GK model, assumes an infinite microelectrode and the 500-μm-diam microelectrode was the one that most closely matched that assumption. Measurements with larger microelectrodes are not convenient. For a circular microelectrode of diameter d_e, the constriction resistance is $\rho/2d_e$, while impedance associated with the microelectrode-cell interface

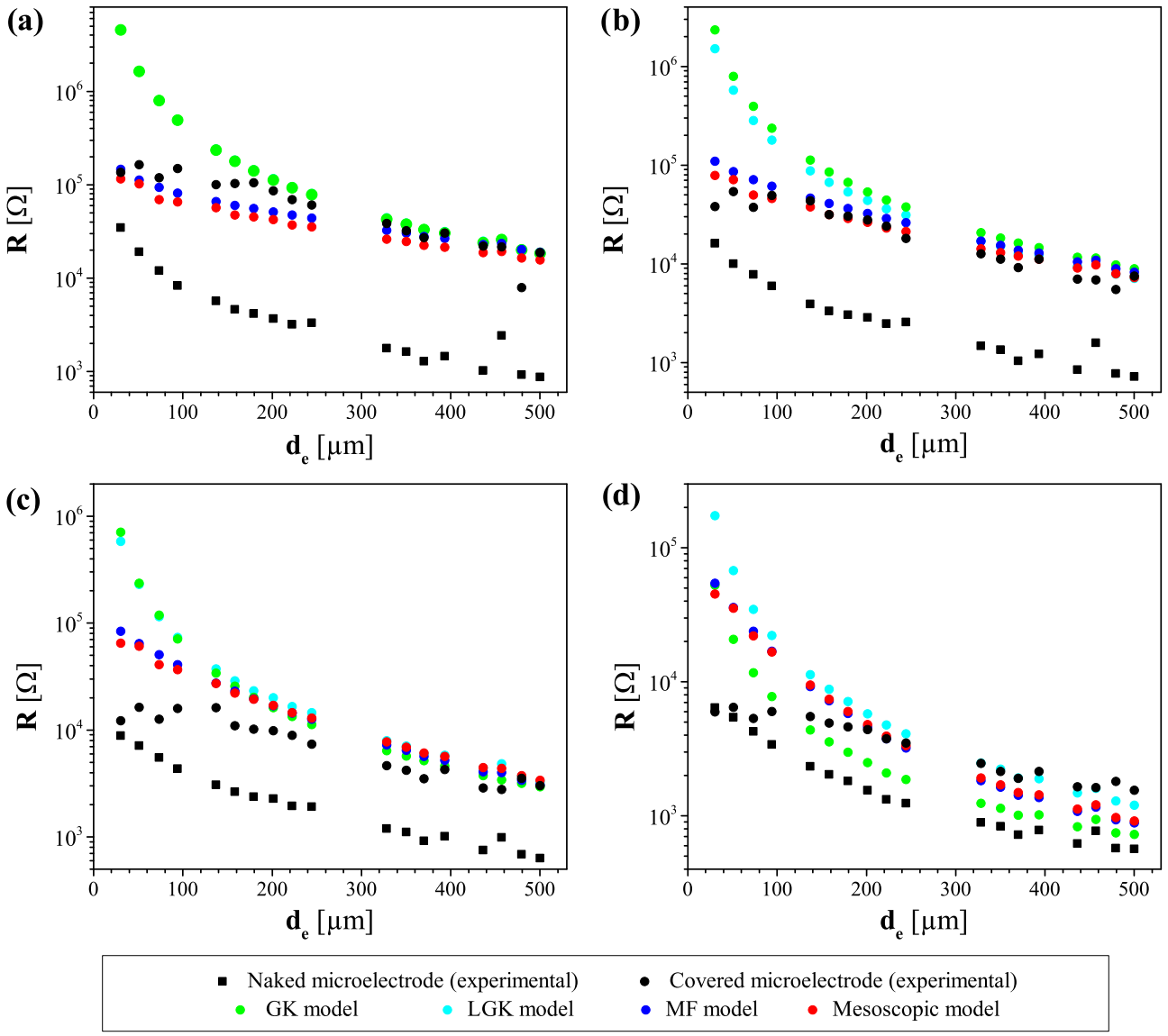

FIG. 8. Experimental resistances of the naked (black squares) and the covered microelectrodes (black circles) and those calculated with the GK (green), MF (blue), and mesoscopic (red) models for the covered microelectrodes with the parameters corresponding to the 500-μm-diam microelectrode. The resistance R is plotted as a function of the microelectrode diameter d_e at frequencies of (a) 1204 Hz, (b) 3492 Hz, (c) 10 125 Hz, and (d) 50 000 Hz.

is inversely proportional to the area of the microelectrode at the frequencies of interest, $4/\pi d_e^2$. If the microelectrode is not small enough, the constriction resistance is dominant and the information that can be extracted about the attached cells is limited. In addition, this assumption was sustained by the choice of a large counter electrode for the measurements, so the impedance of the microelectrode is dominant compared to the impedance of the counter electrode. The counter electrode used had a diameter of 4000 μm, so its area (1.26×10^7 μm^2) was 64 times larger than the area of the largest microelectrode available (500 μm diameter) and 17 778 times larger than the area of the smallest microelectrode (30 μm diameter).

With the parameters corresponding to the 500-μm diameter and the experimental impedances of the other naked microelectrodes, we computed the impedances of the covered microelectrodes and compared them with the experimental data. Figures 8 and 9 show the graphs obtained for resistance and capacitance as a function of the microelectrode diameter for frequencies of 1204 Hz [Figs. 8(a) and 9(a)], which is approximately the frequency of the maximum effect of cells on resistance, 3492 Hz [Figs. 8(b) and 9(b)], 10 125 Hz [Figs. 8(c) and 9(c)], and 50 000 Hz [Figs. 8(d) and 9(d)], which is the frequency of the maximum effect of cells on capacitance. Black squares represent the experimental data of naked microelectrodes, black circles indicate the experimental data of covered microelectrodes, and green, blue, and red circles correspond to the GK, the MF, and the mesoscopic models' data, respectively. In the mesoscopic model, $t_{\text{ins}} = 250$ μm. We observed that the mesoscopic model is the one that best predicts the experimental results and is in excellent agreement with experimental data. The GK model differs significantly from the experimental data for small-radius microelectrodes, although it is worth noting that it provides good

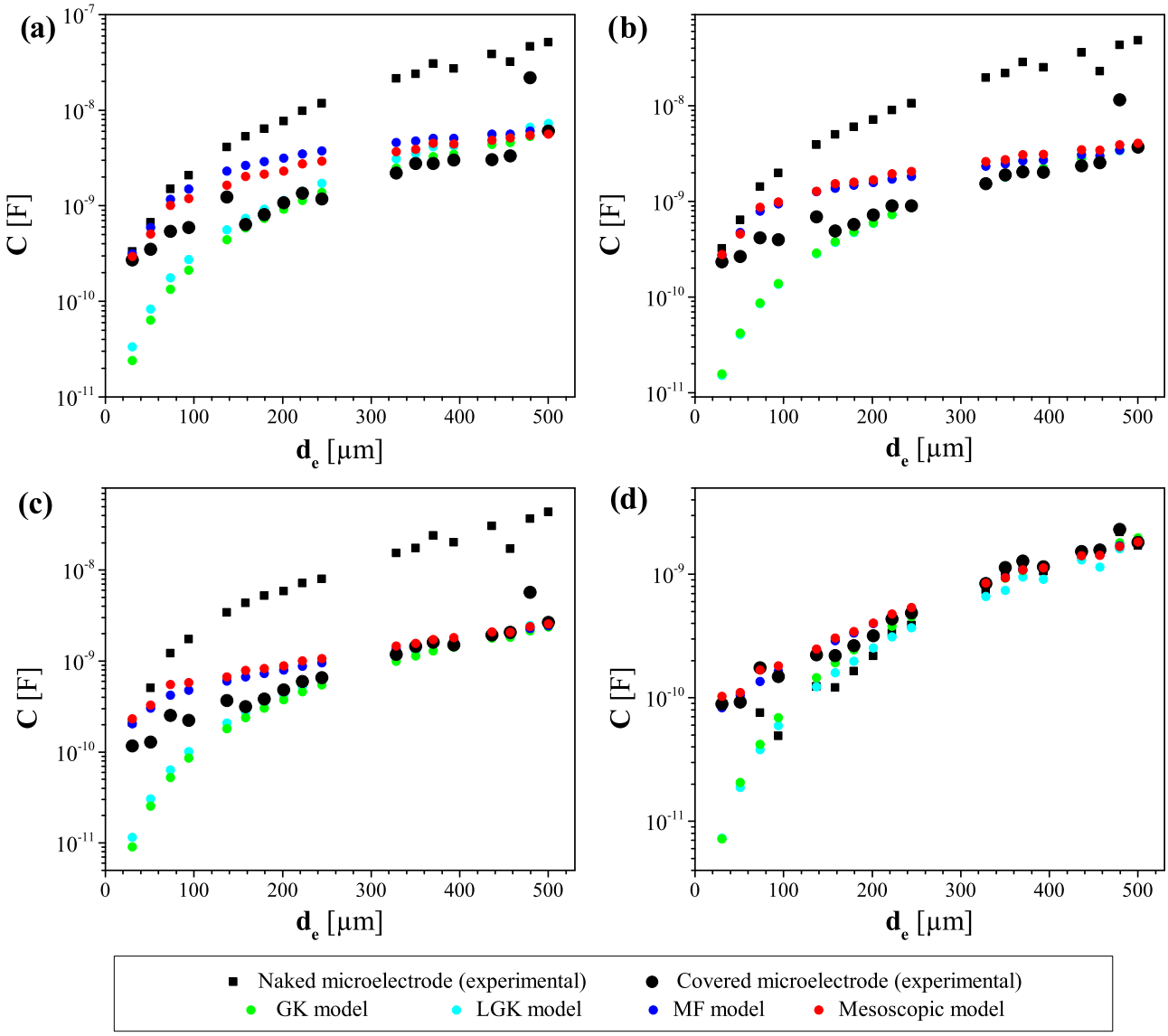

FIG. 9. Experimental capacitances of the naked (black squares) and the covered microelectrodes (black circles) and those calculated with the GK (green), MF (blue), and mesoscopic (red) models for the covered microelectrodes with the parameters corresponding to the 500-μm-diam microelectrode. The capacitance C is plotted as a function of the microelectrode diameter d_e at frequencies of (a) 1204 Hz, (b) 3492 Hz, (c) 10 125 Hz, and (d) 50 000 Hz.

results for 250-μm-diam microelectrodes, which are the most popular size of commercial microelectrodes. At 1204 Hz, the GK model reproduces the experimental resistance with an average difference of 30%, the LGK model with 34%, the MF model with 30%, and the mesoscopic model with 37%, for the range of diameters from 150 to 500 μm. At 50 000 Hz, the GK model differs on average from the experimental capacitance by 9%, the LGK model by 23%, the MF model by 12%, and the mesoscopic model by 13% for the same range of diameters. The most extreme case is the smallest microelectrode (30 μm diameter): The measured resistance of the covered microelectrode at 1204 Hz is 135 kΩ, while the calculate one is 4541 kΩ with the GK model, 4513 kΩ with the LGK model, 146 kΩ with the MF model and 114 kΩ with the mesoscopic model and the experimental capacitance at 50 000 Hz is 0.089 nF, while the calculated one is 0.007 nF with the GK model, 0.007 nF with the LGK model, 0.083 nF with the MF model, and 0.103 nF with the mesoscopic model. In other words, the GK model agrees with the experimental resistance at 1204 Hz with an error of 3263% and with the capacitance at 50 000 Hz with 92%; the errors for the LGK model are 3242% and 92%, respectively, 8% and 7% for the MF model, and 15% and 15% for the mesoscopic model. The percentage errors presented before only consider resistance or capacitance for a single frequency. When considering the impedances for both frequencies, the mesoscopic model presents a lower χ^2 than the other models: χ^2 is 1.3×10^5 for the GK model, 2×10^5 for the LGK model, 1.5×10^4 for the MF model, and 9.8×10^3 for the mesoscopic model. Thereby, the mesoscopic model represents the ECIS data in a wide range of microelectrode radii. One set of parameters fits reasonably well the resistances and capacitances of the

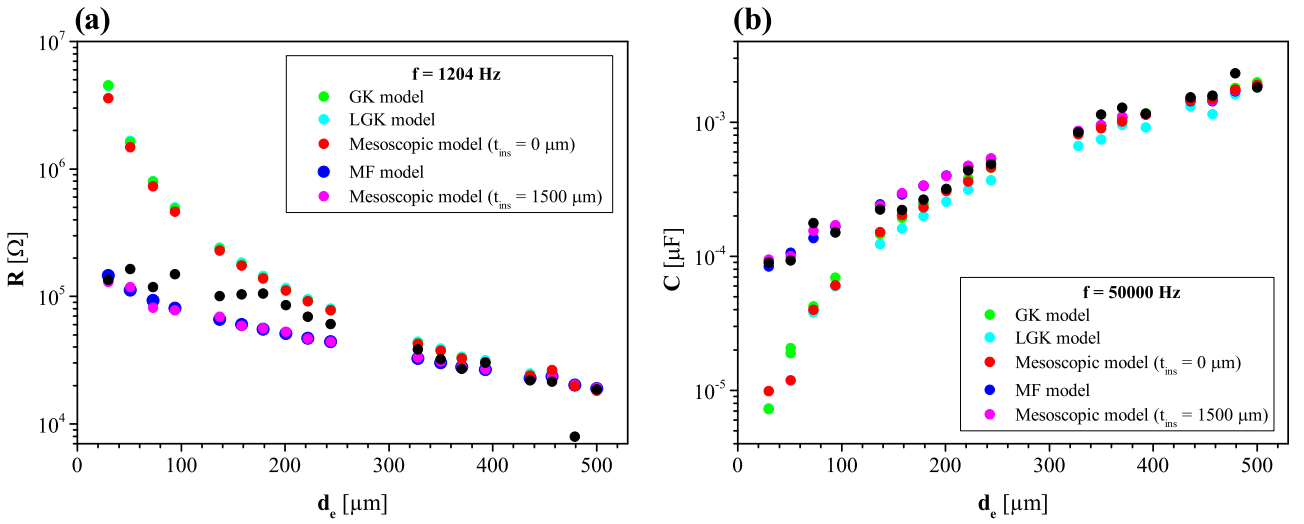

FIG. 10. Experimental (a) resistance at 1204 Hz and (b) capacitance at 50 000 Hz of covered microelectrodes (black) and those calculated with the GK model (green), the MF model (blue), and the mesoscopic model considering an insulator of $t_{\text{ins}} = 0$ μm (red) and $t_{\text{ins}} = 1500$ μm (magenta). The mesoscopic model reduces to the GK model when no insulator is considered and to the MF model when considering an infinite insulator for practical purposes.

covered microelectrodes in the whole range of radii, despite the dependence of the parameters (particularly R_b) on the size of the microelectrode, which is discussed later in the paper.

We recognized two scales in the ECIS system: the microscale that corresponds to the cell radius and the macroscale that corresponds to the microelectrode radius. The existing models to date, the GK, LGK, and MF models, focus on a single scale of the problem. The GK model is derived from electrical balances of a single cell and considers an infinite microelectrode for the boundary condition set (and thus considers no insulator). The MF model takes into account the size of the microelectrode but views cells as a layer with average properties that covers a finite microelectrode and an infinite insulator. In this context, we proposed the mesoscopic model, which simultaneously includes the microscale and the macroscale of the problem. It considers a finite microelectrode and a finite insulator covered by a cell monolayer made up of a central cell surrounded by cell rings coupled to each other. The monolayer does not have average electrical properties as in the MF model, but has properties derived from the individual behavior of the cells that compose it.

Unlike the other two models, the mesoscopic model takes into account an insulator of finite size. Figure 10 shows the experimental resistance at 1204 Hz and capacitance at 50 000 Hz of covered microelectrodes (black) and those calculated with the GK model (green), the MF model (blue), and the mesoscopic model considering an insulator of $t_{\text{ins}} = 0$ μm (red) and $t_{\text{ins}} = 1500$ μm (magenta). We found that the distance between the microelectrode and the electrical ground is relevant, although it had not been taken into account in previous models. We observed that when the size of the insulator is varied in the mesoscopic model, the results of the GK model are recovered if no insulator is considered and those of the MF model are recovered if an infinite insulator (for practical purposes) is considered. In this way, the mesoscopic model has a more general characteristic than the GK and MF models, since these two are extreme cases of the mesoscopic model.

The parameters of the GK model ($\alpha = 34.97\ \Omega^{1/2}$ cm, $R_b = 24.11\ \Omega\,\text{cm}^2$, and $C_m = 2.05\ \mu\text{F/cm}^2$) and those of the mesoscopic model with no insulator ($\alpha = 42.70\ \Omega^{1/2}$ cm, $R_b = 25.38\ \Omega\,\text{cm}^2$, and $C_m = 1.98\ \mu\text{F/cm}^2$) are approximated, since α is slightly greater in this model. Although there is agreement in the covered impedances calculated by the mesoscopic model with an infinite insulator and the MF model, the parameters of both models are not comparable. The values of junction resistance R_b and membrane capacitance C_m in the mesoscopic model have direct biophysical interpretation, unlike the counterparts of the MF model, R_{cells} and C_{cells}, respectively, which do not. While the values of the membrane capacitance C_m are typical and coincide with those estimated with the other models, we observe that the values of R_b are not consistent with values obtained independently.

Next we fitted the GK, mesoscopic, and MF models to the experimental data corresponding to each microelectrode. We did not consider the LGK model in this instance, since its performance is similar to that of the GK model but, unlike this one, it has six adjustable parameters, making a comparison with the other three models impossible.

Figure 11 shows the parameters α, R_b, and C_m provided by the GK and mesoscopic models and ρ/h, R_{cells}, and C_{cells} given by the MF model as a function of the diameter of the microelectrode. We observed a dependence of the parameters on the microelectrode radius. The parameters should not depend on the size of the microelectrode, since, on the one hand, they represent biophysical properties and characteristics of the cells analyzed and, on the other hand, the cells grow on the biocompatible substrate independently of the radius of the microelectrode it contains. In fact, the cell monolayer we analyzed in this set of experiments was the same for every microelectrode, since all the microelectrodes are in the same

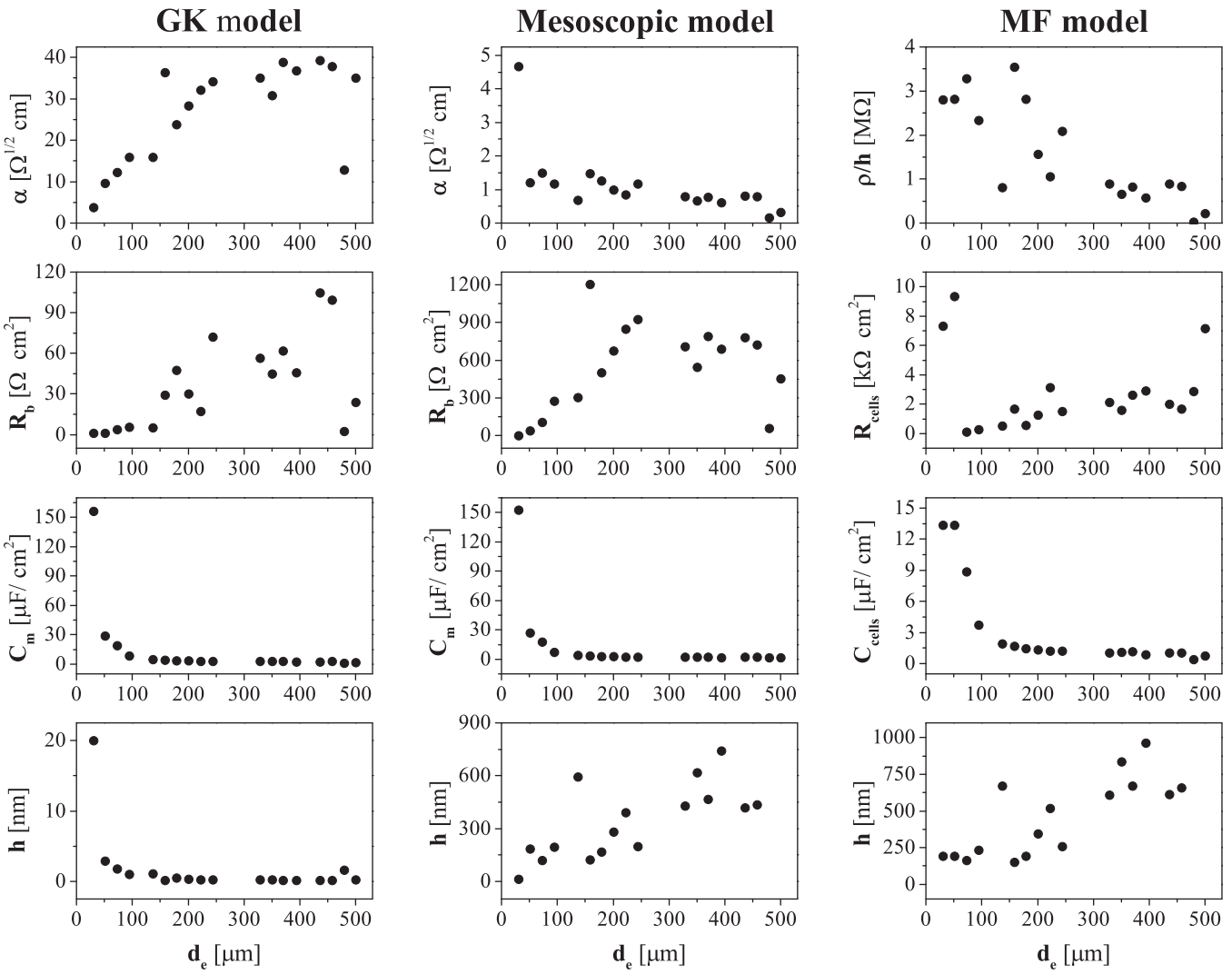

FIG. 11. Parameters obtained with the GK and mesoscopic models (α, R_b, and C_m) and with the MF model (ρ/h, R_{cells}, and C_{cells}) as a function of the microelectrode diameter d_e. The height of the cell-substrate space h estimated from α and ρ/h is also shown.

well (micro-Petri dish) covered by different parts of the same monolayer.

Of particular interest are the parameters α of the GK and mesoscopic models and ρ/h of the MF model, since they are associated with the height of the substrate-cell space h. This is important for the analysis and definition of other cellular properties [15–18]. Figure 11 also shows the estimated value of h. We noticed that h varies greatly from one model to another: It is in the range between 0.2 and 3 nm in the GK model and the median of h is (610 ± 60) nm for the MF model and (420 ± 40) nm for the mesoscopic model. With the GK model, h is so small that it is not realistic and it is significantly larger with the MF model. The mesoscopic model estimates a value of h in the intermediate range, closer to that obtained in measurements recorded in the literature (15–150 nm) [19–26]. The distance between the substrate and the basal cell membrane h estimated with the mesoscopic model is larger than the maximum value measured directly (150 nm). We hypothesize that the difference may be due to the fact that the direct measurements of h were performed with cells cultivated on pretreated glass or plastic, while we measured cells grown on gold. Nevertheless, the height ($h = 0.3$ nm) estimated with the GK model from the data of the 500-μm-diam microelectrode, in concordance with the infinite microelectrode size assumption, is $\frac{1}{50}$ of the minimum value measured directly (15 nm).

We also noticed a correlation between the parameters R_b of the GK and mesoscopic models and R_{cells} of the MF model that increases with the radius of the microelectrode and a correlation between C_m of the GK and mesoscopic models and C_{cells} of the MF model that decreases with the radius. It is worth noting that the mesoscopic model is less sensitive to variations in R_b than to variations in α. Although R_b varies considerably over the range of microelectrode sizes used, α improves remarkably, allowing estimates of heights of the substrate-cell space h in the range of what is optically observed, unlike the other models.

V. CONCLUSION

In this paper, we proposed, presented, and validated an analytical model, the mesoscopic model, which represents

an advance in the description of the problem of ECIS. This model manages to simultaneously consider the two scales of the problem, which correspond to the size of a cell (microscale) and the size of the microelectrode and the insulator (macroscale).

We made a critical comparison between the existing models (the Giaever-Keese, Lo-Giaever-Keese, and mean field models) and the mesoscopic model, analyzing the effect of the microelectrode radius from each model, using experimental data obtained by applying the ECIS technique to monolayers of MDCK II cells grown on microelectrodes of different sizes. We showed that the mesoscopic model is the one that best predicts the experimental results. Despite the dependence of the parameters on the radius of the microelectrodes, we showed that this model represents the experimental data for a wide range of radii.

For the current standard model, the GK model, a single set of parameters is not enough to represent the experimental data in the entire range of microelectrode diameters. Although the GK model provides excellent results for the bigger microelectrodes, we noticed that results predicted for the smaller microelectrodes differ significantly from the experimental data.

In this way, it has been established that the infinite microelectrode assumption of the GK model precludes the correct analysis of the experimental data obtained with small microelectrodes and the mesoscopic model arises as a versatile and accurate alternative. Since the use of small microelectrodes (of sizes comparable to those of a cell or even smaller) is of huge relevance in the study of heterogeneous cultures, having a model capable of functioning properly in this size range is of the utmost importance. Heterogeneous cultures are conformed by islands of different types of cells (for instance, healthy and cancer cells). It is convenient to use electrodes smaller than the islands of cells in order to avoid recording measurements of the borders between islands, which cannot be studied. Thus, the smaller the microelectrode used for measurements, the smaller the islands it can analyze and the better the information it can obtain about the heterogeneous culture. In the most extreme case, when there exist islands of the size of a cell, it would be necessary to map the whole heterogeneous cell monolayer with microelectrodes smaller than the cells.

Although the mesoscopic model represents a small quantitative improvement compared to the mean field model, the most remarkable differences between these two models were found in their approaches. On the one hand, the MF model considers cells as electronic entities (electrical resistances and capacitances), while the mesoscopic model takes into account the biophysical parameters of interest. In addition, the parameters of the mesoscopic model are compatible with and comparable to those of the GK model, the standard model. This represents a significant advantage of the mesoscopic model over the MF model, since the cellular biophysical parameters are of great importance in the characterization of the cells. Thereby, there is a lack of information on the electronic quantities provided by the MF model. For instance, unlike the mesoscopic model, the MF model is not capable of quantifying the resistance of the intercellular junctions R_b, which is a relevant parameter in cell characterization.

On the other hand, the MF model considers an infinite cell monolayer with mean electrical properties that covers a finite microelectrode and an infinite insulator, so it works for a system in which cells have no dimension. In the mesoscopic model, all the physical entities involved (cells, microelectrode, and insulator) are considered finite and the properties of the monolayer are derived from those of an individual cell. Thus, the mesoscopic model is generalizable to an eventually three-dimensional system. In this way, this model allows us to spatially distinguish the rings of cells that conform to the monolayer.

Finally, the most important advantage of the mesoscopic model over the GK and MF models is that the mesoscopic model's approach and the way it is derived may potentially allow us to model heterogeneous cultures, wound-healing processes, etc.

We conclude that the representation of the system achieved by the mesoscopic model is more detailed than that of previous models. The mentioned benefits that this model presents may be valuable for several ECIS applications.

[1] I. Giaever and C. Keese, Monitoring fibroblast behavior in tissue culture with an applied electric field, Proc. Natl. Acad. Sci. U.S.A. **81**, 3761 (1984).

[2] I. Giaever and C. Keese, Use of electric fields to monitor the dynamical aspect of cell behavior in tissue culture, IEEE Trans. Biomed. Eng. **33**, 242 (1986).

[3] I. Giaever and C. Keese, A morphological biosensor for mammalian cells, Nature (London) **366**, 591 (1993).

[4] C. Keese and I. Giaever, A biosensor that monitors cell morphology with electrical fields, IEEE Eng. Med. Biol. Mag. **13**, 402 (1994).

[5] A. Ahuja, M. Behrend, J. Whalen, M. Humayun, and J. Weiland, The dependence of spectral impedance on disc microelectrode radius, IEEE Trans. Biomed. Eng. **55**, 1457 (2008).

[6] Y. Lai, Y. Chu, J. Lo, Y. Hung, and C. Lo, Effects of electrode diameter on the detection sensitivity and frequency characteristics of electric cell-substrate impedance sensing, Sensor. Actuat. B **288**, 707 (2019).

[7] I. Giaever and C. R. Keese, Micromotion of mammalian cells measured electrically, Proc. Natl. Acad. Sci. U.S.A. **88**, 7896 (1991).

[8] C. Lo, C. Keese, and I. Giaever, Impedance analysis of MDCK cells measured by electric cell-substrate impedance sensing, Biophys. J. **69**, 2800 (1995).

[9] E. Urdapilleta, M. Bellotti, and F. J. Bonetto, Impedance analysis of cultured cells: A mean-field electrical response model for electric cell-substrate impedance sensing technique, Phys. Rev. E **74**, 041908 (2006).

[10] M. Bellotti, Evaluación biológica y fisicoquímica de dispositivos ECIS postulados para el diagnóstico de patologías oculares, Ph.D. thesis, Universidad Nacional de Buenos Aires, 2010.

[11] W. Bast, Desarrollo de arreglos de electrodos micromaquinados para aplicaciones en biotecnología, Ph.D. thesis, Universidad Nacional de Cuyo, 2014.

[12] R. Pradhan, A. Mitra, and S. Das, Characterization of electrode/electrolyte interface of ECIS devices, Electroanalysis **24**, 2405 (2012).

[13] D. Price, A. Rahman, and S. Bhansali, Design rule for optimization of microelectrodes used in electric cell-substrate impedance sensing (ECIS), Biosens. Bioelectron. **24**, 2071 (2009).

[14] X. Zhang, W. Wang, A. Nordin, F. Li, S. Jang, and I. Voiculescu, The influence of the electrode dimension on the detection sensitivity of electric cell-substrate impedance sensing (ECIS) and its mathematical modeling, Sensor. Actuat. B **247**, 780 (2017).

[15] C. Lo, C. Keese, and I. Giaever, Cell-substrate contact: Another factor may influence transepithelial electrical resistance of cell layers cultured on permeable filters, Exp. Cell Res. **250**, 576 (1999).

[16] N. Kataoka, K. Iwaki, K. Hashimoto, S. Mochizuki, Y. Ogasawara, M. Sato, K. Tsujioka, and F. Kajiya, Measurements of endothelial cell-to-cell and cell-to-substrate gaps and micromechanical properties of endothelial cells during monocyte adhesion, Proc. Natl. Acad. Sci. U.S.A. **99**, 15638 (2002).

[17] C. Lo, M. Glogauer, M. Rossi, and J. Ferrier, Cell-substrate separation: Effect of applied force and temperature, Eur. Biophys. J. **27**, 9 (1998).

[18] C. Lo and J. Ferrier, Electrically measuring viscoelastic parameters of adherent cell layers under controlled magnetic forces, Eur. Biophys. J. **28**, 112 (1999).

[19] L. Hackett, S. Seo, S. Kim, L. Goddard, and G. Liu, Label-free cell-substrate adhesion imaging on plasmonic nanocup arrays, Biomed. Opt. Express **8**, 1139 (2017).

[20] V. Heitmann, B. Reiß, and J. Wegener, in *Piezoelectric Sensors*, edited by C. Steinem and A. Janshoff, Springer Series on Chemical Sensors and Biosensors Vol. 5 (Springer, Berlin, 2006), pp. 303–338.

[21] J. Burmeister, L. Olivier, W. Reichert, and G. Truskey, Application of total internal reflection fluorescence microscopy to study cell adhesion to biomaterials, Biomaterials **19**, 307 (1998).

[22] J. Burmeister, G. Truskey, and W. Reichert, Quantitative analysis of variable-angle total internal reflection fluorescence microscopy (VA-TIRFM) of cell/substrate contacts, J. Microsc. **173**, 39 (1994).

[23] M. Ward and D. Hammer, A theoretical analysis for the effect of focal contact formation on cell-substrate attachment strength, Biophys. J. **64**, 936 (1993).

[24] H. Verschueren, Interference reflection microscopy in cell biology: Methodology and applications, J. Cell Sci. **75**, 279 (1985).

[25] C. Izzard and L. Lochner, Formation of cell-to-substrate contacts during fibroblast motility: An interference-reflexion study, J. Cell Sci. **42**, 81 (1980).

[26] C. Izzard and L. Lochner, Cell-to-substrate contacts in living fibroblasts: An interference reflexion study with an evaluation of the technique, J. Cell Sci. **21**, 129 (1976).